

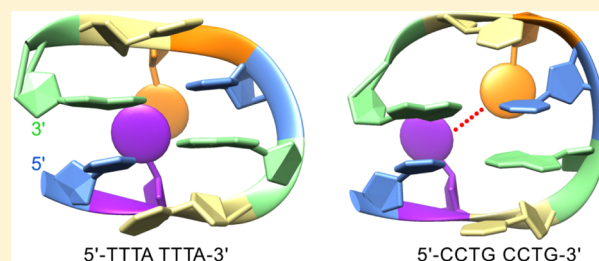
Minidumbbell: A New Form of Native DNA Structure

Pei Guo and Sik Lok Lam*

Department of Chemistry, The Chinese University of Hong Kong, Shatin, New Territories, Hong Kong

S Supporting Information

ABSTRACT: The non-B DNA structures formed by short tandem repeats on the nascent strand during DNA replication have been proposed to be the structural intermediates that lead to repeat expansion mutations. Tetranucleotide TTTA and CCTG repeat expansions have been known to cause reduction in biofilm formation in *Staphylococcus aureus* and myotonic dystrophy type 2 in human, respectively. In this study, we report the first three-dimensional minidumbbell (MDB) structure formed by natural DNA sequences containing two TTTA or CCTG repeats. The formation of MDB provides possible pathways for strand slippage to occur, which ultimately leads to repeat expansion and thus expansion mutations. Our result here shows that MDB is a highly compact structure composed of two type II loops. In addition to the typical stabilizing interactions in type II loops, MDB shows extensive stabilizing forces between the two loops, including two distinctive modes of interactions between the minor groove residues. The formation of MDB enriches the structural diversity of natural DNA sequences, reveals the importance of loop–loop interactions in unusual DNA structures, and provides insights into novel mechanistic pathways of DNA repeat expansion mutations.



INTRODUCTION

DNA is well-known to adopt the right-handed double-helical B-form structure.¹ Over the past five decades, DNA has also been shown to be capable of adopting non-B structures such as A- and Z-form DNA,^{2,3} bubble, hairpin,^{4,5} dumbbell,⁶ three-way junction,⁷ triplex,⁸ sticky DNA,⁹ quadruplex,¹⁰ i-motif,^{11,12} and cruciform.¹³ These non-B structures have been demonstrated to participate in various biological processes such as gene regulation, DNA replication, transcription, damage, and repair. In particular, the non-B structures adopted by short tandem repeats in the nascent strand during DNA replication, e.g., CTG hairpin,⁵ GAA triplex,¹⁴ CGG quadruplex,¹⁵ GCC i-motif,¹² and CCTG dumbbell,⁶ have been proposed to be the culprits leading to repeat expansion mutations^{16–18} which bring about nearly 30 human genetic disorders.¹⁷ Meanwhile, non-B structures have also become fascinating building blocks in DNA nanotechnology and material science owing to their unique structural features.^{19,20}

Recently, we showed that two TTTA²¹ or CCTG repeats²² are capable to fold into a minidumbbell (MDB) structure, which not only provides possible pathways for the occurrence of TTTA and CCTG repeat expansions in *Staphylococcus aureus* and myotonic dystrophy type 2 patients, respectively, but also enriches the structural diversity of natural DNA sequences. The MDB structure comprises two tetranucleotide type II loops with 3'-5' terminal stacking. In a type II loop,^{23–25} the first and fourth loop residues form a loop-closing base pair whereas the second and third residues fold into the minor groove and stack on the base pair, respectively. Yet how two adjacent type II loops in a single DNA strand lead to the formation of MDB remains elusive. Therefore, we have determined the three-

dimensional solution structures of TTTA and CCTG MDBs in this study. Our results reveal these MDBs are highly compact with extensive stabilizing interactions between the two loops. We have also identified two distinctive modes of stabilization between the minor groove residues.

MATERIALS AND METHODS

This section only provides a brief description of key materials and experimental methods. The detailed experimental procedures are described in [Supporting Information](#) (SI) Materials and Methods.

DNA Samples. The two DNA samples used in this study contain the sequence 5'-TTTA TTTA-3' and 5'-CCTG CCTG-3', respectively. For simplicity, these two DNA samples were named as "(TTTA)₂" and "(CCTG)₂". NMR samples were prepared by dissolving 0.5 μmol of purified DNA into 500 μL buffer solutions containing 10 mM sodium phosphate (pH 7.0), and 0.1 mM 2,2-dimethyl-2-silapentane-5-sulfonic acid.^{21,22}

NMR Spectroscopy. The details of NMR experiments and resonance assignments are described in [Supporting Information](#). To extract the nonlabile proton NOEs, the samples were prepared in a 99.96% D₂O buffer solution, and 2D NOESY spectra were acquired with mixing times of 100, 300, and 600 ms at 5 °C unless otherwise specified. To study the labile protons, the solvent was exchanged with a 90% H₂O/10% D₂O buffer solution. The 2D NOESY and 1D NOE difference spectra were acquired using the excitation sculpting water suppression method.²⁶ For the measurements of the ³J_{H1'H2'}, ³J_{H4'H5'}, and ³J_{H4'H5''} coupling constants, DQF-COSY spectra were acquired.

Experimental Restraints. Proton–proton distance restraints were obtained from NOESY spectra based on the intensities of NOE cross peaks. A total of 242 and 274 distance restraints were obtained for

Received: July 4, 2016

Published: September 2, 2016

(TTTA)₂ and (CCTG)₂, respectively. Besides, distance restraints based on crystallographic data for hydrogen bonds in Watson–Crick T–A and C–G base pairs²⁷ were used. The H1'–C1'–C2'–H2' sugar torsion angles were determined by the ³J_{H1'H2'} coupling constants measured from the DQF-COSY spectra and the Karplus equation.²⁸ Glycosidic torsion angles χ were obtained based on the intranucleotide H6/H8–H1' NOE intensities. Restraints for backbone torsion angles γ were determined based on the analysis of ³J_{H4'H5'/H5''} coupling constants.²⁹ A summary of the restraints used in calculating the structures of (TTTA)₂ and (CCTG)₂ is shown in Tables S1 and S2.

Structure Calculations. Restrainted molecular dynamics (rMD) calculations were performed using AMBER³⁰ with the ff12SB force field.³¹ See the protocol in Support Information.

Data Analysis. The pseudorotation phase angles (P) of deoxyribose puckers were measured using the CPPTRAJ module of AMBER 12.³² The criteria of hydrogen bond and hydrophobic interaction are stated in Support Information. All figures of the calculated structures were generated using UCSF Chimera.³³

RESULTS AND DISCUSSION

Overview of the TTTA MDB Solution Structure. For (TTTA)₂, 20 refined structures with lowest restraint violation energies were selected in the final representative ensemble (PDB ID: 5GWQ). Superimposition of them shows the TTTA MDB structure was well-defined with reasonable precision (Figure 1A). Specifically, the first and fourth loop residues, i.e., T1 and A4, and T5 and A8, form the loop-closing base pairs. The second loop residues, namely T2 and T6, fold into the minor groove and partially stack with each other whereas the third loop residues T3 and T7 stack on T1–A4 and T5–A8 base pairs, respectively. Among the 20 structures, the average pairwise RMSD was found to be 0.87 ± 0.20 Å and the RMSD from the mean structure was 0.60 ± 0.14 Å for all residues (Table 1). All these structures show (i) satisfactory agreement with experimental restraints with no large distance and torsion angle violations and (ii) good covalent geometries with no significant bond and angle violations (Table 1). The backbone and glycosidic torsion angles and pseudorotation phase angles are summarized in Figure S1.

The Core Scaffold of TTTA MDB Was Constructed by Two Watson–Crick Loop-Closing Base Pairs with 3'–5' Terminal Stacking. The core scaffold was constructed by two well-defined loop-closing T–A base pairs with an average pairwise RMSD of 0.78 ± 0.20 Å (Table 1). The T1–A4 and T5–A8 base pairs adopt Watson–Crick pairing geometry with an extensive stack between the A8 and T1 termini (Figure 1B). As supported by the 1D NOEs of A4/A8 H2 but not H8 by saturating the T1/T5 imino signals at ~13.5 ppm (Figure S2A,B), Watson–Crick hydrogen bond restraints were added in the structural refinement process to increase the chance of obtaining the structures with lowest restraint violation energy. To verify the Watson–Crick pairing modes, we also repeated the structural refinement process by removing these hydrogen bond restraints. Among 100 rMD trials with random starting velocities, the structure with lowest restraint violation remains an MDB with two T–A Watson–Crick base pairs (Figure S2C).

As the observed Watson–Crick base pairings differ from the Hoogsteen pairings found in the TTTA loop of hairpin^{23,34} and TTCA loop of cyclic DNA,³⁵ we again repeated the structural refinement by incorporating Hoogsteen hydrogen bond restraints to avoid underestimating the possibility of forming Hoogsteen loop-closing base pairs. Among 100 trials, the lowest restraint violation energy was found to be about 6-fold higher than that with Watson–Crick hydrogen bond restraints.

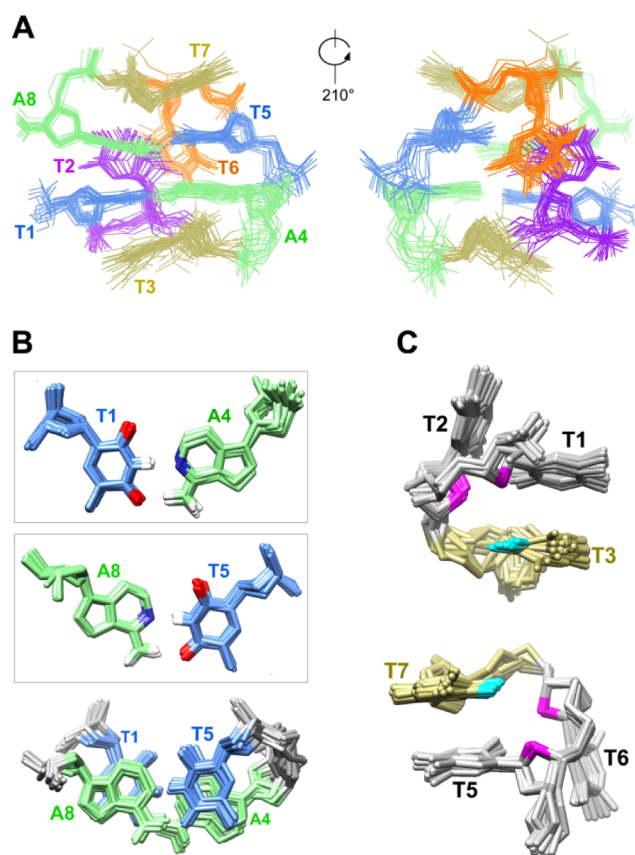


Figure 1. MDB structure of (TTTA)₂. (A) The major and minor groove views of 20 superimposed structures of (TTTA)₂. The third loop residues T3 and T7 stack on the T1–A4 and T5–A8 loop-closing base pairs while the second loop residues T2 and T6 fold into the minor groove and partially stack with each other. (B) T1–A4 and T5–A8 form the Watson–Crick loop-closing base pairs (top) with extensive base–base stacking (bottom). (C) Hydrophobic interactions were observed between T3/T7 methyl (cyan) and the 2'–methylene groups (magenta) of its two preceding residues.

The results of the above two tests support the Watson–Crick pairing geometry in the two loop-closing base pairs in TTTA MDB. Together with the extensive 3'–5' terminal stack (Figure 1B), as supported by the base–base NOEs between A8 and T1 (Figure S3A), these loop-closing base pairs provide substantial stabilization in constructing the core scaffold of TTTA MDB.

The Third Loop Residues Show Stacking and Hydrophobic Interactions. In type II TTTA loops, the third thymine residue stabilizes the loop through stacking with the loop-closing base pair.^{23,34} In TTTA MDB, T3 and T7 were also found to stack on the loop-closing base pairs (Figure 1A). These stacking interactions are supported by the base–base NOEs including T3 H7–T1 H6, T3 H6–A4 H2, T7 H7–T5 H6, and T7 H6–A8 H2 (Figure S3A). It has been suggested that the formation of a Hoogsteen instead of Watson–Crick loop-closing base pair would provide better stacking for the third residue in type II loop due to the shorter C1'–C1' distance.^{23,24,36} However, it is apparent that the 3'–5' terminal stack between the two Watson–Crick loop-closing base pairs is more crucial toward the formation of TTTA MDB. As a result, the stacking interactions between T1–A4 and T5–A8 Watson–Crick base pairs outweigh the enhanced stabilizing effects of T3 on T1–A4 and T7 on T5–A8 Hoogsteen base pairs, making T–A

Table 1. NMR and Refinement Statistics

	(TTTA) ₂	(CCTG) ₂
Structural Restraints		
number of distance restraints		
inter-residue	103	82
intraresidue	139	192
hydrogen bond	4	6
subtotal	246	280
number of torsional restraints		
lycosidic (χ)	8	8
sugar (H1'-C1'-C2'-H2')	2	4
backbone (γ)	3	5
subtotal	13	17
Restraint Satisfaction		
distance restraints (Å)		
number of violations >0.2 Å	1.6 ± 0.9	0.6 ± 0.7
maximum violation	0.26	0.25
average violation	0.09 ± 0.06	0.08 ± 0.05
torsional restraints (deg)		
number of violations >5°	0	0
maximum violation	0.7	0
average violation	0.6 ± 0.1	0
Deviations from Covalent Geometry		
bonds (Å)	0.0086 ± 0.0002	0.0100 ± 0.0003
angles (deg)	2.5 ± 0.1	2.5 ± 0.1
Heavy Atomic RMSD (Å) ^a		
all residues		
average pairwise RMSD	0.87 ± 0.20	1.06 ± 0.28
RMSD from mean structure	0.60 ± 0.14	0.73 ± 0.19
loop-closure base pairs		
average pairwise RMSD	0.78 ± 0.20	0.77 ± 0.24
RMSD from mean structure	0.54 ± 0.10	0.54 ± 0.15

^aPairwise RMSD was calculated among 20 refined structures.

Watson–Crick base pairs more favorable than T-A Hoogsteen base pairs in TTTA MDB.

Apart from base–base stacking, the sugars of the third loop residues T3 and T7 also directly stack on A4 and A8 of the loop-closure base pairs, respectively (Figure 1A), as supported by the more upfield chemical shifts of the H1', H2', and H2'' sugar protons than those of other residues (Table S3). In addition, hydrophobic interactions were also observed between the methyl group of T3 or T7 and the 2'-methylene groups of its two preceding residues (Figure 1C). In these hydrophobic cores, the distances from T3 C7 to T1 C2'/T2 C2' and from T7 C7 to T5 C2'/T6 C2' were found to be 3.4 ± 0.1 Å/ 4.7 ± 0.2 Å, and 3.6 ± 0.1 Å/ 5.4 ± 0.2 Å, respectively. In general, the hydrophobic interaction involving T3 or T7 with its second preceding residue was found to be stronger than that with its first preceding residue.

Folding of T2 and T6 into the Minor Groove. In TTTA MDB, both of the second loop residues T2 and T6 were folded into the minor groove, with T2 being closer to the loop-closure base pairs than T6 (Figure 1A). Their relative positions are supported by (i) the presence of NOEs between T2 and A4/A8 and (ii) the absence of NOEs between T6 and A4/A8 (Figure S3B). Among the 20 refined structures, five show a T2 H3-T5 O2 hydrogen bond (Figure 2A), nine show a T2 H3-T7 O5' hydrogen bond (Figure 2B), and six show a T2 H3-T7 OP1 hydrogen bond (Figure 2C). These indicate that the folding of T2 into the minor groove was driven by the formation of hydrogen bond between T2 imino and the loop-closure base pair T5 O2 or the phosphodiester backbone T7 O5'/OP1 of the second TTTA repeat. Owing to the stabilization between T2 and T5/T7, the loop formed by the second repeat was more well-defined than the loop formed by the first repeat (Figure 2A–C), as evidenced by a much smaller average pairwise RMSD of 0.61 ± 0.16 Å for the second repeat than that of 0.89 ± 0.23 Å for the first repeat.

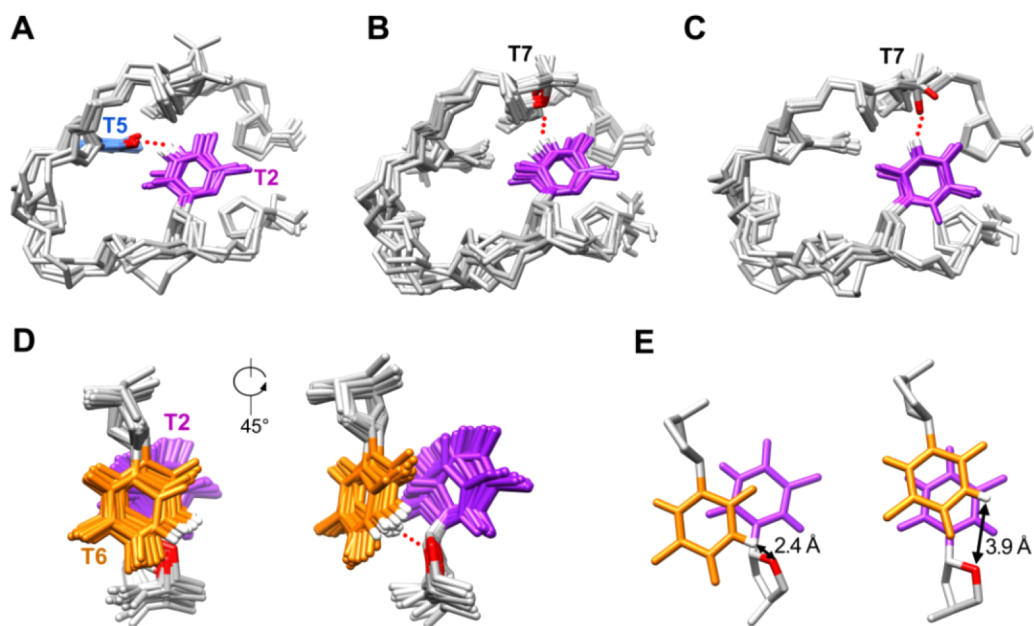


Figure 2. Stabilizing interactions involving the minor groove T2 and T6 residues. (A) Five structures show a T2 H3-T5 O2 hydrogen bond with a bond length of 2.2 ± 0.4 Å. (B) Nine structures show a T2 H3-T7 O5' hydrogen bond with a bond length of 2.9 ± 0.3 Å. (C) Six structures show a T2 H3-T7 OP1 hydrogen bond with a bond length of 2.1 ± 0.6 Å. (D) T6 stacks with T2 (left). An additional T6 H3-T2 O4' hydrogen bond was observed with a bond length of 2.8 ± 0.4 Å (right). (E) A stronger T6 H3-T2 O4' hydrogen bond was observed in the case that T2 and T6 were not well-stacked (left). With better stacking, the T6 H3-T2 O4' hydrogen bond was found to be weaker (right).

Instead of a hydrogen bond, the folding of T6 into the minor groove was predominantly driven by base–base stacking with T2 (Figure 2D). This stacking geometry is supported by the NOEs of T2 H7–T6 H1' and T2 H1'–T6 H7 (Figure S3B). In addition to this minor groove residues' stack which has also been observed in cyclic DNA,³⁵ an unprecedented T6 H3–T2 O4' hydrogen bond was found to complement the base–base stacking in the minor groove (Figure 2D). Pending the degree of stacking overlap between T2 and T6, the length of this hydrogen bond was found to vary from 2.4 to 3.9 Å in the 20 refined structures (Figure 2E).

Overview of the CCTG MDB Solution Structure. Similarly, 20 refined structures of (CCTG)₂ with lowest restraint violation energies were selected in the final representative ensemble (PDB ID: 5GWL). The core scaffold of CCTG MDB was also well-defined by the two loop-closure base pairs (Figure 3A) with an average pairwise RMSD of 0.77 ± 0.24 Å (Table 1). CCTG MDB shows some structural similarities to TTTA MDB, including (i) two Watson–Crick loop-closure base pairs (Figure 3B) as supported by the NOEs between G4/G8 imino and C1/C5 amino protons (Figure S4A), (ii) the 3'-5' terminal stack (Figure 3B) as supported by the base–base NOEs of C1 H6–G8 H8 and C1 H5–G8 H8

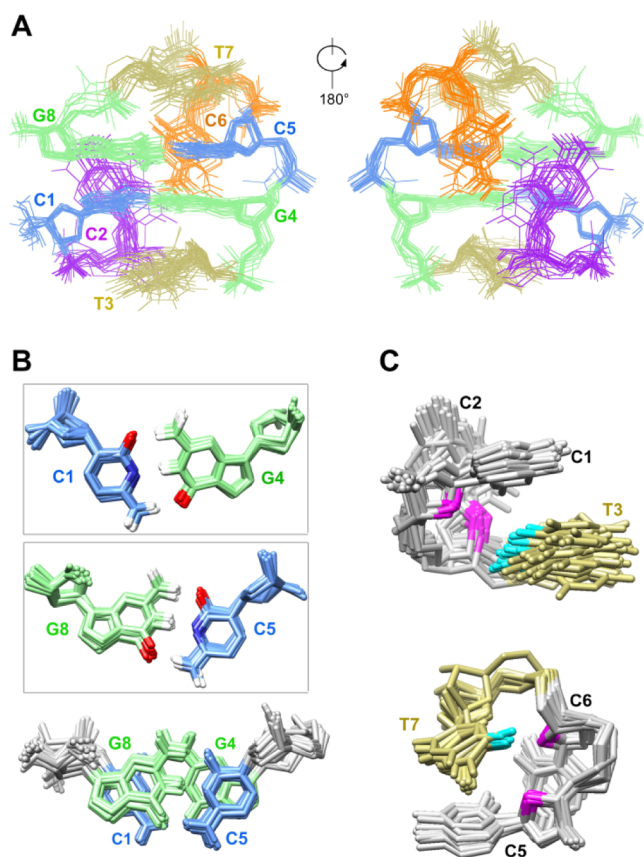


Figure 3. MDB structure of (CCTG)₂. (A) The major and minor groove views of 20 superimposed structures of (CCTG)₂. The third loop residues T3 and T7 stack on the C1–G4 and C5–G8 loop-closure base pairs, while the second loop residues C2 and C6 fold into the minor groove and pair up with multiple geometries. (B) C1–G4 and C5–G8 form the Watson–Crick loop-closure base pairs (top) and stack extensively with each other (bottom). (C) Hydrophobic interactions were observed between T3/T7 methyl (cyan) and the 2'-methylene groups (magenta) of its two preceding residues.

(Figure S4B), (iii) the stacking of the third loop residues on the base pairs (Figure 3A) as supported by the base–base NOEs between T3 and C1, and between T7 and C5 (Figure S4B) and the more upfield T3/T7 H1', H2', and H2'' sugar proton chemical shifts (Table S3). Stabilizing hydrophobic interactions were also found between the methyl group of T3 or T7 and the 2'-methylene groups of its two preceding residues (Figure 3C). The backbone and glycosidic torsion angles and pseudorotation phase angles are summarized in Figure S5.

Exchangeable Pairing Geometries of C–C Mismatch in the Minor Groove of CCTG MDB. In CCTG MDB, the second loop residues C2 and C6 were also folded into the minor groove. However, instead of stacking with each other, C2 and C6 were found to pair up with six different geometries via hydrogen bond(s) and/or Na⁺-mediated electrostatic interaction(s) (Figure 4A). These include (i) 13 cases showing a C2 O2–C6 H41 hydrogen bond with C2 O2/N3...Na⁺...C6 O2/N3 electrostatic interactions, (ii) two showing a C2 O2–C6 H41 hydrogen bond without Na⁺-mediated electrostatic interaction, (iii) two showing only C2 O2/N3...Na⁺...C6 O2/N3 electrostatic interactions, (iv) one showing a C2 H41–C6 O2 hydrogen bond, (v) one showing a C2 H41–C6 N3 hydrogen bond, and (vi) one showing C2 N3–C6 H41 and C2 H41–C6 N3 hydrogen bonds. As suggested by the seriously broadened C2 and C6 H6 signals (Figure S4C), there is conformational exchange among these pairing geometries. Owing to these multiple C2–C6 pairing geometries, a relatively larger average pairwise RMSD of 1.06 ± 0.28 Å for all residues was obtained (Table 1).

The exchange between different pairing geometries can occur via hydrogen bond(s) breaking/forming and/or the addition/removal of Na⁺-mediated electrostatic interaction(s). It is reasonable that we observed more simple hydrogen bond pairing geometries in the refined structures, as they are involved in the conformational exchange pathways between the one containing two hydrogen bonds and the one containing no hydrogen bonds. For the pairing geometry with a C2 O2–C6 H41 hydrogen bond and C2 O2/N3...Na⁺...C6 O2/N3 electrostatic interactions (Figure 4A, i), it occurs more frequently than the others probably because it is involved in more conformational exchange pathways. This pairing geometry can be formed from the one with only a C2 O2–C6 H41 hydrogen bond (Figure 4A, ii) by simply gaining Na⁺-mediated electrostatic interactions or from the one with C2 O2/N3...Na⁺...C6 O2/N3 electrostatic interactions (Figure 4A, iii) by forming a C2 O2–C6 H41 hydrogen bond.

In addition to the pairing interactions between C2 and C6, hydrogen bonding interactions were also found between C2/C6 and the loop-closure base pairs or the phosphodiester backbone to assist the folding of C2 and C6 into the minor groove in CCTG MDB. For the most frequently observed C2–C6 pairing geometry which shows a C2 O2–C6 H41 hydrogen bond and Na⁺-mediated electrostatic interactions (Figure 4A, i), two to three hydrogen bonds were usually formed with the loop-closure base pairs via C2 O2–G4/G8 H22, C2 N3–G8 H22 (Figure 4B, left), and/or C6 H42–G4 N3 (Figure 4C, left), and two to three hydrogen bonds with the phosphodiester backbone via C2 H41/H42–G8/OP1/OP2/O4'/O5' (Figure 4B, right) and/or C6 H42–T3 OP1 (Figure 4C, right), indicating both of the minor groove residues are capable of forming hydrogen bonds with the loop-closure base pairs and backbone. For the C2–C6 pairing geometry with two symmetric hydrogen bonds (Figure 4A, vi), three additional hydrogen

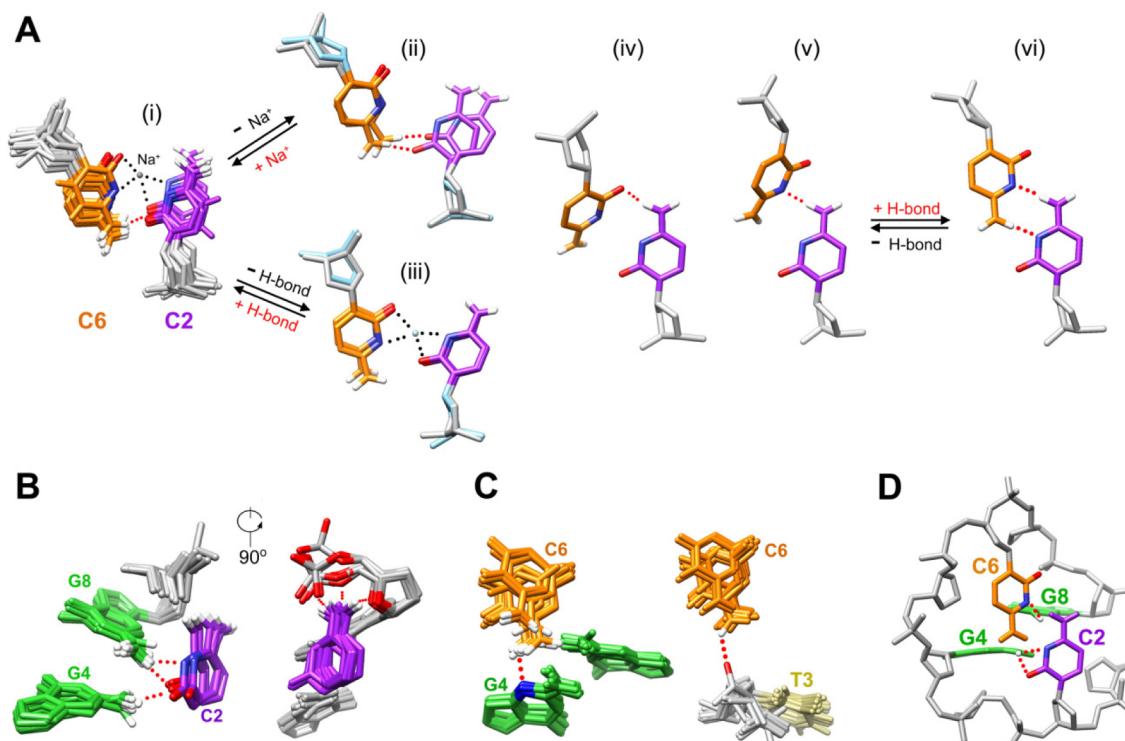


Figure 4. Multiple C2-C6 pair geometries in CCTG MDB. (A) Six C2-C6 pair geometries were observed, including (i) a C2 O2-C6 H41 hydro en bond and Na⁺-mediated C2 O2/N3...Na⁺...C6 O2/N3 electrostatic interactions, (ii) C2 O2-C6 H41 hydro en bond, (iii) Na⁺-mediated C2 O2/N3...Na⁺...C6 O2/N3 electrostatic interactions, (iv) C2 H41-C6 O2 hydro en bond, (v) C2 H41-C6 N3 hydro en bond, and (vi) two symmetric C2 N3-C6 H41 and C2 H41-C6 N3 hydro en bonds. These pair geometries are interconvertible by simply breaking/forming hydro en bond(s) and/or losing/gaining Na⁺-mediated electrostatic interactions. Arrows were added between the pair geometries that differed by one hydro en bond or the presence/absence of Na⁺-mediated electrostatic interactions. In the pair geometry with C2 O2-C6 H41 hydro en bond and Na⁺-mediated electrostatic interactions, (B) C2 and (C) C6 form additional hydro en bonds with the loop-closing base pair and the phosphodiester backbone. (D) In the pair geometry with two symmetric hydro en bonds, C2 and C6 can only form hydro en bonds with the loop-closing base pairs.

bonds were formed with the loop-closing base pairs via C2 O2/N3-G4 H22 and C6 N3-G8 H22 but not the backbone (Figure 4D).

Loop-Loop Interactions in TTTA and CCTG MDBs.

The presence of extensive stabilizing interactions makes the folding of an 8-nt DNA strand into a highly compact MDB structure feasible. In TTTA and CCTG MDBs, these stabilizing interactions include (i) 3'-5' terminal stacking between the two loop-closing base pairs, (ii) stacking between the third loop residues with the loop-closing base pairs, (iii) hydrophobic interactions between the third loop residues with their two preceding residues, (iv) base-base stacking and/or pairing interactions between the two minor groove residues, and (v) hydro en bonds between the minor groove residue with the loop-closing base pair/phosphodiester backbone. Among them, there are extensive loop-loop interactions overlying the MDB structure. These loop-loop interactions are absent in the larger dumbbell structure.⁶ In TTTA MDB, T1 and A4 in the first loop shows extensive base-base stacking with A8 and T5, respectively, and the minor groove T2 in the first loop stacks with T6 and forms hydro en bonds with T5, T6, and T7 (Figure 5A). In CCTG MDB, in addition to the stacking between the two loop-closing base pairs, C2 forms hydro en bonds with C6 and G8 in the second loop, and C6 forms hydro en bonds with T3 and G4 in the first loop (Figure 5B).

Loop-loop interactions have been shown to be biologically important in nucleic acids. In RNA, loop-loop interactions are involved in the formation of a kissing complex which serves as

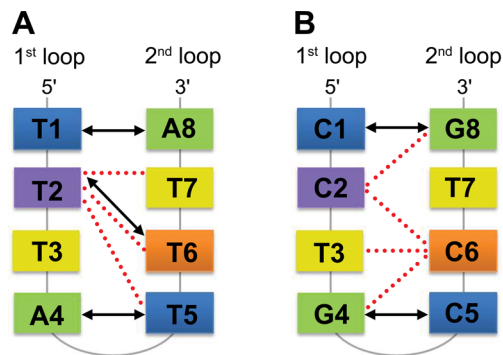


Figure 5. Loop-loop interactions in TTTA and CCTG MDBs. (A) The loop-loop interactions observed in TTTA MDB include (i) the stacking between T1-A4 and T5-A8 loop closing base pairs, (ii) hydro en bonds between T2 and T5/T6/T7, and (iii) base-base stacking between T2 with T6. (B) For CCTG MDB, these include (i) the stacking between C1-G4 and C5-G8 base pairs, (ii) hydro en bonds between C2 and C6/G8, and (iii) hydro en bonds between C6 and T3/G4. The stacking and hydro en bond interactions are represented by black arrows and red dotted lines, respectively.

an intermediate step in the dimerization of the RNA genomes of the human immunodeficiency virus³⁷ and the hepatitis C virus.³⁸ In DNA, loop-loop interactions have been shown to participate in CAG and CTG repeat expansion mutations.³⁹ More efficient mismatch repair escape was observed in the presence of adjacent CAG/CTG slip-outs than simple slip-out,

reveal the significance of loop–loop interactions between adjacent slip-outs.⁴⁰ Recently, loop–loop interactions in DNA–DNA kissing complexes have been used in the nanotechnology area to construct tetrahedrons.⁴¹ In TTTA and CCTG MDBs, these extensive loop–loop interactions play a crucial role in maintaining the structures, providing insights into the underlying chemical forces which bring about strand slippage in TTTA and CCTG repeats during DNA replication.

Biological Significance of MDBs. The formation of MDB in the nascent strand during DNA replication can lead to variable sizes of repeat expansions.^{21,22} First, MDB can be formed via a slippage of two TTTA or CCTG repeats in the nascent strand. This provides a possible pathway for the occurrence of two-repeat expansion. Second, it has been shown that two competing MDBs can be formed in a segment of three repeats, including one with a 5'-overhang in repeat and one with a 3'-overhang in repeat.^{21,22} Fast exchange between these two MDBs results in the formation of a miniloop, which can lead to one-repeat expansion. Third, coexistence of multiple MDBs and/or miniloops can also occur in the nascent strand, resulting in three-repeat or larger size expansion.

For repeat expansions to occur, the above MDBs and miniloops formed in the nascent strand must escape from DNA repair. To achieve this, conformational exchange between the MDBs and/or miniloops can take place, which provides a potential pathway to avoid the specific recognition by DNA repair proteins. For TTTA and CCTG MDBs, their reported melting temperatures are 18.1 °C and 22.2 °C, respectively.^{21,22} These temperatures reveal an optimized thermodynamic stability for feasible formation of MDBs and occurrence of conformational exchange, thus bring about TTTA and CCTG repeat expansions during DNA replication.

■ ASSOCIATED CONTENT

Supporting Information

The Supporting Information is available free of charge on the ACS Publications website at DOI: 10.1021/jacs.6b06897.

Materials and methods section; additional experimental data (Tables S1–S3 and Figures S1–S6) (PDF)

■ AUTHOR INFORMATION

Corresponding Author

*lams@cuhk.edu.hk

Notes

The authors declare no competing financial interest.

■ ACKNOWLEDGMENTS

We thank Professor H. N. C. Wong for his continuous support of the research activities of our group. The work described in this paper was supported by General Research Fund (project nos. CUHK14302114 and CUHK14302915) and Special Equipment Grant (project no. SEG/CUHK09) from the Research Grants Council of the Hong Kong Special Administrative Region.

■ REFERENCES

- (1) Watson, J. D.; Crick, F. H. *Nature* **1953**, *171*, 737.
- (2) DiMaio, F.; Yu, X.; Rensen, E.; Krupovic, M.; Pranshvil, D.; Egelman, E. H. *Science* **2015**, *348*, 914.
- (3) Pohl, F. M.; Jovin, T. M. *J. Mol. Biol.* **1972**, *67*, 375.
- (4) Bikard, D.; Loot, C.; Baharolu, Z.; Mazel, D. *Microbiol. Mol. Biol. Rev.* **2010**, *74*, 570.

- (5) Chi, L. M.; Lam, S. L. *Nucleic Acids Res.* **2005**, *33*, 1604.
- (6) Lam, S. L.; Wu, F.; Yan, H.; Chi, L. M. *Nucleic Acids Res.* **2011**, *39*, 6260.
- (7) van Buuren, B. N.; Overmars, F. J.; Ippel, J. H.; Altona, C.; Wijmen, S. S. *J. Mol. Biol.* **2000**, *304*, 371.
- (8) Asensio, J. L.; Brown, T.; Lane, A. N. *Structure* **1999**, *7*, 1.
- (9) Sakamoto, N.; Chastain, P. D.; Parniewski, P.; Ohshima, K.; Pandolfo, M.; Griffith, J. D.; Wells, R. D. *Mol. Cell* **1999**, *3*, 465.
- (10) Phan, A. T.; Kuryavyi, V.; Luu, K. N.; Patel, D. J. *Nucleic Acids Res.* **2007**, *35*, 6517.
- (11) Kovanda, A.; Zalar, M.; Sket, P.; Plavec, J.; Roelj, B. *Sci. Rep.* **2015**, *5*, 17944.
- (12) Kaushik, M.; Suehl, N.; Marky, L. A. *Biophys. Chem.* **2007**, *126*, 154.
- (13) Brazda, V.; Laister, R. C.; Jalska, E. B.; Arrowsmith, C. *BMC Mol. Biol.* **2011**, *12*, 33.
- (14) Gacy, A. M.; Goellner, G. M.; Spiro, C.; Chen, X.; Gupta, G.; Bradbury, E. M.; Dyer, R. B.; Mikesell, M. J.; Yao, J. Z.; Johnson, A. J.; Richter, A.; Melancon, S. B.; McMurray, C. T. *Mol. Cell* **1998**, *1*, 583.
- (15) Adrian, M.; An, D. J.; Lech, C. J.; Heddi, B.; Nicolas, A.; Phan, A. T. *J. Am. Chem. Soc.* **2014**, *136*, 6297.
- (16) Buard, J.; Bourdet, A.; Yardley, J.; Dubrova, Y.; Jeffreys, A. J. *EMBO J.* **1998**, *17*, 3495.
- (17) Mirkin, S. M. *Nature* **2007**, *447*, 932.
- (18) Zhou, K.; Aertsen, A.; Michiels, C. W. *FEMS Microbiol. Rev.* **2014**, *38*, 119.
- (19) Jones, M. R.; Seeman, N. C.; Mirkin, C. A. *Science* **2015**, *347*, 1260901.
- (20) Choi, J.; Majima, T. *Chem. Soc. Rev.* **2011**, *40*, 5893.
- (21) Guo, P.; Lam, S. L. *FEBS Lett.* **2015**, *589*, 1296.
- (22) Guo, P.; Lam, S. L. *FEBS Lett.* **2015**, *589*, 3058.
- (23) Blommers, M. J.; van de Ven, F. J.; van der Marel, G. A.; van Boom, J. H.; Hilbers, C. W. *Eur. J. Biochem.* **1991**, *201*, 33.
- (24) Ippel, H. H.; van den Elst, H.; van der Marel, G. A.; van Boom, J. H.; Altona, C. *Biopolymers* **1998**, *46*, 375.
- (25) Cho, S. H.; Chin, K. H.; Chen, C. W. *J. Biomol. NMR* **2001**, *19*, 33.
- (26) Stott, K.; Stonehouse, J.; Keeler, J.; Hwang, T. L.; Shaka, A. J. *J. Am. Chem. Soc.* **1995**, *117*, 4199.
- (27) Saenger, W. *Principles of Nucleic Acid Structure*; Springer: New York, 1984.
- (28) Altona, C.; Sundaralingam, M. *J. Am. Chem. Soc.* **1972**, *94*, 8205.
- (29) Wijmen, S. S.; van Buuren, B. N. M. *Prog. Nucl. Magn. Reson. Spectrosc.* **1998**, *32*, 287.
- (30) Case, D. A.; Cheatham, T. E., III; Darden, T.; Gohlke, H.; Luo, R.; Merz, K. M., Jr.; Onufriev, A.; Simmerling, C.; Wang, B.; Woods, R. J. *J. Comput. Chem.* **2005**, *26*, 1668.
- (31) Perez, A.; Marchan, I.; Svozil, D.; Sponer, J.; Cheatham, T. E., III; Lauhtonen, C. A.; Orozco, M. *Biophys. J.* **2007**, *92*, 3817.
- (32) Roe, D. R.; Cheatham, T. E., III. *J. Chem. Theory Comput.* **2013**, *9*, 3084.
- (33) Pettersen, E. F.; Goddard, T. D.; Huang, C. C.; Couch, G. S.; Greenblatt, D. M.; Menon, E. C.; Ferrin, T. E. *J. Comput. Chem.* **2004**, *25*, 1605.
- (34) Blommers, M. J.; Walters, J. A.; Haasnoot, C. A.; Aelen, J. M.; van der Marel, G. A.; van Boom, J. H.; Hilbers, C. W. *Biochemistry* **1989**, *28*, 7491.
- (35) Escaja, N.; Gomez-Pinto, I.; Rico, M.; Pedroso, E.; Gonzalez, C. *ChemBioChem* **2003**, *4*, 623.
- (36) van Dongen, M. J.; Wijmen, S. S.; van der Marel, G. A.; van Boom, J. H.; Hilbers, C. W. *J. Mol. Biol.* **1996**, *263*, 715.
- (37) Paillart, J. C.; Skripkin, E.; Ehresmann, B.; Ehresmann, C.; Marquet, R. *Proc. Natl. Acad. Sci. U. S. A.* **1996**, *93*, 5572.
- (38) Shetty, S.; Kim, S.; Shimakami, T.; Lemon, S. M.; Mihailescu, M. R. *RNA* **2010**, *16*, 913.
- (39) Pearson, C. E.; Wang, Y. H.; Griffith, J. D.; Sinden, R. R. *Nucleic Acids Res.* **1998**, *26*, 816.
- (40) Panirahi, G. B.; Slean, M. M.; Simard, J. P.; Gileadi, O.; Pearson, C. E. *Proc. Natl. Acad. Sci. U. S. A.* **2010**, *107*, 12593.

(41) Barth, A.; Kobbe, D.; Focke, M. *Nucleic Acids Res.* **2016**, *44*, 1502.